Geometry Influence on the Location of Incipient Cracking of Pipe Bends under In-plane Bending

K. Kussmaul, H. Diem, E. Roos, D. Uhlmann
Staatliche Materialprüfungsanstalt, University of Stuttgart,
Federal Republic of Germany

Third International Conference on Biaxial/Multiaxial Fatigue,
Stuttgart, April 3 to 6, 1989

Abstract

In-plane bending of pipe bends generates a complex load-dependent biaxial state of stress which controls the failure history. It is shown in the paper that the deformation behavior of pipe bends depends on geometry. In 90° bends, the dominant parameter is the ratio of the outer to the inner diameters. In thin-walled bends, shell type bending dominates, i.e., there is pronounced ovalization with the points of maximum load being situated on the inner surface in the region of the bend flanks. In thick-walled bends, prismatic bending dominates with the peak being situated on the intrados on the outside of the bend. Under a sufficient number of cyclic load changes, thin-walled bends develop longitudinal cracks on the inside of the bend, while thick-walled bends fail as a result of a circumferential crack on the outside.

1 Introduction

Pipe bends are among the most important components of pipe systems. They are dimensioned as a function of the installation requirements necessary to achieve pipe isometry and the requirements imposed by the process involved. In general, they are designed in accordance with the provisions of applicable codes on the basis of internal pressure and maximum stress limitation as a

function of the safety criteria to be met.

Because of their lower stiffness, compared to the straight pipe sections which precede or follow them, pipe bends are used to absorb by elastic deformation the forces and moments of reaction within a system. If pipe systems are exposed to elevated temperatures, the pipe bends serve to convert into bending moments and bending strains, respectively, the thermal expansions of straight pipe sections. Bending moments produce deformations of cross section (ovalization) in pipe bends, which can give rise to local strain concentrations at certain points on the shell of a bend. If such processes are repeated, as is the case, e.g., when a plant is started up and shut down several times or when dynamic loads are applied, there may be incipient cracking followed by crack growth up to failure of a component.

The large variety of pipe bend geometries, wall thicknesses, large or small radii of curvature, large or small bend opening angles raises the question where on the shell of the bend the highest loads will occur and, as a consequence, give rise to cracking under cyclic loads.

2 Pipe Bend Characterization

In general, pipe bends are characterized in terms of the bend coefficient,

$$\lambda = \frac{R}{r_m} \frac{t}{r_m}$$

and the shell parameter, $\frac{t}{r_m}$. The diameter ratio, u, and the shell parameter can be transformed into each other,

$$u = \frac{D_o}{D_i} = \frac{2 + \frac{t}{r_m}}{2 - \frac{t}{r_m}}$$

and therefore are equally well suited to characterize the thin- or thick-walled nature of a bend. In boiler and piping design, the limit, u = 1,2 /1/ is used to distinguish thin or thick walls.

The broad range of pipe bends manufactured by the cold forming technology /2/ or by the mandrel bending process /3/ have bend coefficients between 0,1 and 2 and diameter ratios between 1,02 and 1,5. Induction type bending, however, /4/ can attain λ-values of up to 50 and diameter ratios of up to 2,3.

The terms chosen and the definition of the angles used are summarized in Fig. 1.

2.1 Deformation Behavior of Pipe Bends

In this chapter, the characteristic deformation behavior of 90° pipe bends with straight pipe sections connected on both sides is described under in-plane bending load conditions without internal pressure in the range of linear elastic materials behavior. This means that no influence of the material and no influence of the operating temperature need to be taken into account in these considerations, as both parameters only affect the absolute stress and strain levels, respectively.

In-plane bending loads applied to pipe bends without internal pressure cause more or less pronounced cross sectional deformation in the region of the bend. The external bending load in the meridian direction is superimposed by a shell type bending load in the circumferential direction, which results in a biaxial stress condition in the region of the bend. The transition from the uniaxial stress condition in the straight pipe legs to the multiaxial stress condition in the bend and in the pipe regions influenced by the bend occurs by way of shear stresses.

With in-plane bending, a basic distinction must be made between bending in opening mode and bending in closing mode. The

fundamental strain distribution to the inner and the outer surfaces, which occurs in the apical cross section, is shown qualitatively in Fig. 2. The only difference between the inward and outward bending load cases is a reversal of the signs of the stress and strain distributions, respectively.

The example of three pipe bend geometries loaded in static in-plane bending tests can be used to demonstrate the influence of the geometry on the deformation behavior. The characteristic data of these bends are listed in Table 1. It should be noted that the characteristic parameters indicated have been calculated from mean values determined experimentally, but the real bends exhibit major or minor variations in wall thickness and outer diameter both over the circumference and along the meridian lines.

Fig. 3 to 5 show equivalent strain distributions on the outer and inner surfaces of the apex of the bend for the three bend geometries selected. The reference strains were calculated from measured single strain values by the relation

$$\varepsilon_{eq} = \frac{1}{1-\mu^2}\sqrt{(1-\mu+\mu^2)(\varepsilon_t^2+\varepsilon_a^2) + (4\mu-1-\mu^2)\varepsilon_t\varepsilon_a}$$

and normalized to the peak level encountered in the respective cross section. The strain values measured only at discrete points on the shell of the bend were connected mathematically in third degree polygonal treatment in order to allow the strain behavior to be interpreted from the closed curve traces. It becomes evident at this point that in no case the point of maximum load was covered directly by the choice of the measuring positions. The positions of maximum load determined analytically therefore carry some uncertainty as a result of interpolation which, however, is of no great significance with respect to the further described findings.

Comparison of the three bend geometries shows that the

thin-walled bend (A) experiences its highest load on the inner surface in the region of the bend flanks (φ=90° and 270°), respectively). In the type B bend geometry, there are two other zones with relatively high stresses on the inner and outer surfaces of the intrados (φ=180°) in addition to the points of maximum load on the side of the bend. The extremely thick-walled type C bend shows three points under approximately the same stress, one on the outside of the intrados, and another on one the inside in the region of the bend flanks. The pictures show clearly that, as the wall thickness increases, another point of high stress arises on the intrados on the outside of the bend, in addition to the points of high stress on the sides of the bend. The extrados, however, always remains a region of relatively low stress level.

2.2 Positions of Potential Sites of Incipient Cracking

Under cyclic loading of the bends in the range of linear elastic materials behavior, the same reference strain distributions arise qualitatively as are shown in Fig. 3 to 5, with the only difference that the ordinates now must be denoted $2\varepsilon_a$. In this way, the points on the shell of the bend can be indicated for the three bend geometries at which cracking can occur under fatigue, Fig. 6. The positions in brackets denote zones with delayed incipient cracking as a consequence of a lower strain amplitude.

Another interesting point is the question of the orientation of the crack nuclei produced. To answer it, the individual strain components - axial strain, ε_a, and circumferential strain, ε_t, are shown for the inner and the outer surfaces in Fig. 7 to 9. In thin-walled type A bends, the circumferential strain dominates in the region of the bend flanks, i.e., cracking will have an axial orientation. In type B bends, the circumferential strain dominates on the inside while, on the outside, the axial strain exceeds the circumferential strain by a very slight margin. In this case, longitudinal cracks along the sides of the bend must

be expected to occur first on the inside. Because of the lower strain amplitude, there may be a longitudinal crack on the inside of the intrados and a circumferentially oriented crack on the outside of the intrados after some delay. In thick-walled type C pipes, axial strain dominates on the outside and circumferential strain on the inside. In this case, crack nuclei can arise nearly at the same time on the intrados and and on the sides of the bend, which will be circumferentially oriented on the intrados and axially oriented in the region of the sides of the bend.

3 Tests on the Incipient Cracking Behavior of Bends

In a number of fatigue tests, four type A pipe bends with nominal widths between DN 80 and DN 400 and one type C bend were loaded in cyclic bending tests starting from the undamaged component and passing through incipient cracking up to failure. Three of the tests were run on the pipe test rig assembled on the clamping plate of MPA Stuttgart, a schematic diagram of which is shown in Fig. 10 /5/. The pipe system consisted of a main conduit of a nominal width of DN 250 and a bypass conduit of a nominal width of DN 80, both of which were attached to the test structure at one fixed point each.

In two tests, the pipe system and the pipe bends under study, Fig. 11, were made of austenitic niobium stabilized X 10 CrNiNb 18 9 steel. In the tests, the bypass conduit was always rearranged as a function of the required wall thickness of the bend. The bends to be studied were welded in place at position X (cf. Fig. 12).

The pipe system loaded in the tests, in the presence of varying levels of internal pressure, by a cyclic vertical force, F_z, essentially produced a cyclic in-plane bending moment at the bends under study; minor out-of-plane components caused by the type of force application were negligible. All tests were

conducted at room temperature and used tap water as the pressurizing medium.

As a consequence of the high cyclic load, incipient cracking of the components was found at the positions expected from strain measurements in geometrically similar bends (cf. Section 2.1).

The most important data of the tests performed on the two pipe bends are summarized in Table 2. As the time available for the tests was limited, the tests were run at strain amplitudes in the range of hyperelastic materials behavior. It should be noted that the strain level indicated on the inside of the thin-walled bend is only an approximation estimated from finite element results, as no strain measurements were conducted on the inner surface in this test.

The thin-walled bend failed by producing a leakage through a longitudinal crack in the side of the apex of the bend, Fig. 12. The first crack initiation occurred in the area of the bend flanks on the inside of the wall; in the course of the test, however, there was additional crack initiation on the outside of the wall (also in the longitudinal direction, cf. Fig. 12).

Unlike the thin-walled bend, the thicker-walled component failed from a leakage caused by a circumferential crack, Fig. 13. The crack initiated on the outside of the wall on the intrados of the middle of the bend and grew preferentially in the direction of the wall thickness. This component developed delayed longitudinal cracking in the region of the bend flanks, which had grown to a depth of 60 % of the wall thickness by the end of the test.

In two other tests involving in-plane bending in thin-walled pipe bends ($u \sim 1{,}14 - 1{,}18$), which were conducted within the HDR Safety Program, also longitudinal cracks were produced in the region of the sides of the bends /6, 7/. It was seen that the

characteristic deformation behavior of this type of bend always gives rise to a crack field (cf. examples in Fig. 14 and 15) extending practically over the whole length of the bend. In the course of time, a macrocrack develops from this crack field which finally controls the mode of failure.

4 Summary

In-plane bending of elbows generates a biaxial state of stress within the bend by a load-dependent change of the cross-sectional shape. I could by shown in static and cyclic tests of pipe bends of various geometries that the deformation and failure behavior of pipe bends is a function of geometry. The parameter chosen to describe this dependence was the ratio between the outer and inner diameters. As the D_o/D_i ratio increases, the zones of maximum stress move from the sides of the bend to the intrados. Under cyclic load, thin-walled bends produce crack fields with aixally oriented cracks on the inner surface of the sides of the bend, while thick-walled bends develop circumferentially oriented cracks on the outside of the intrados. The transition region from thin to thick walls in 90° bends is at a diameter ratio of 1,2. The location of incipient cracking is controlled by the maximum equivalent strain whereas the orientation of the cracks depends on the maximum single strain.

5 References

/1/ DIN 2413, Stahlrohre,
Berechnung der Wanddicke gegen Innendruck

/2/ Product Range of Cold Formed Pipe Bends
Fa. KVF GmbH, Kaarst, FRG

/3/ Product Range of Pipe Bends Manufactured by the Mandrel Process,
Fa. Siekmann Fittings GmbH, Lohne, FRG

/4/ Product Range of Inductive Bends,
Fa. Deutsche Babcock Werke AG, Oberhausen, FRG

/5/ Diem, H., Beißwänger, F., Müller, K.U., Jansky, J.:
Investigation on Stressing and Failure of Pipe Elbows,
PHDR-Report No.: 56-84, February 1985

/6/ Diem, H., Uhlmann, D., Mikkola, T.J., Hunger, H.:
Ergebnisse von Rohrversagensversuchen bis zum Durchriß im zylindrischen Rohrteil RORV(A) und im Krümmerbereich RORV(B),
11. Statusbericht, HDR Sicherheitsprogramm, Karlsruhe, Dezember 1987

/7/ Diem, H., Malcher, L.:
Rohrleitungsversuche mit vorgeschädigten Komponenten unter überhöhter, erdbebenähnlicher Belastung und Betriebsbedingungen,
12. Statusbericht, HDR-Sicherheitsprogramm, Karlsruhe, Dezember 1988

Table 1: Characteristic geometrical data of the pipe bends under investigation in static tests

	u	λ	R/r_m	DN
Bend A	1,16	0,44	2,94	120
Bend B	1,21	0,86	4,41	400
Bend C	1,39	1,0	3,07	80

Table 2: Main data of the pipe bends under investigation in fatigue tests

Dimensions D_o [mm]	t	R	Material	Strain range $[10^{-3}\ \frac{m}{m}]$	Internal pressure [MPa]	Number of load cycles until incipient cracking	Total number of load cycles until failure	Failure mode	Failure position	Failure orientation
88,8	5,6	115	X 10 CrNiNb 18 9	7,2	10	2200	3650	leakage	bend flank	longitudinal
118	16	152	X 10 CrNiNb 18 9	5	16	8000	10000	leakage	intrados	circumferential
				11			1107 } 11107			

Staatliche Materialprüfungsanstalt

Universität Stuttgart

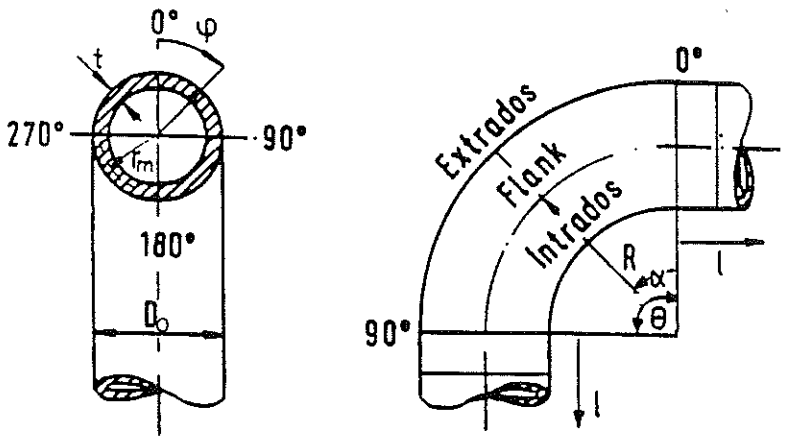

Fig. 1: Notation and angle convention

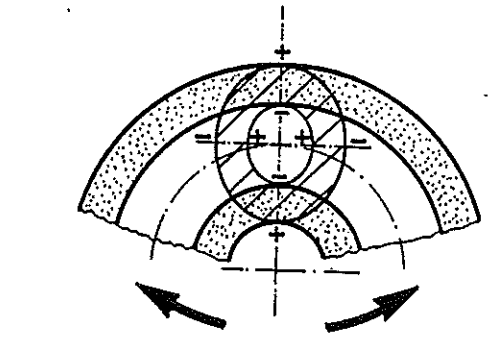

+ Tension

− Compression

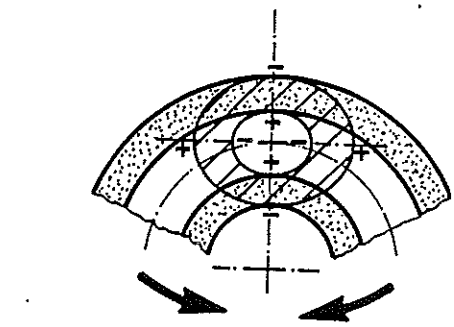

Fig. 2: Schematic representation of pipe bend ovalization under in-plane bending

Staatliche Materialprüfungsanstalt

Universität Stuttgart

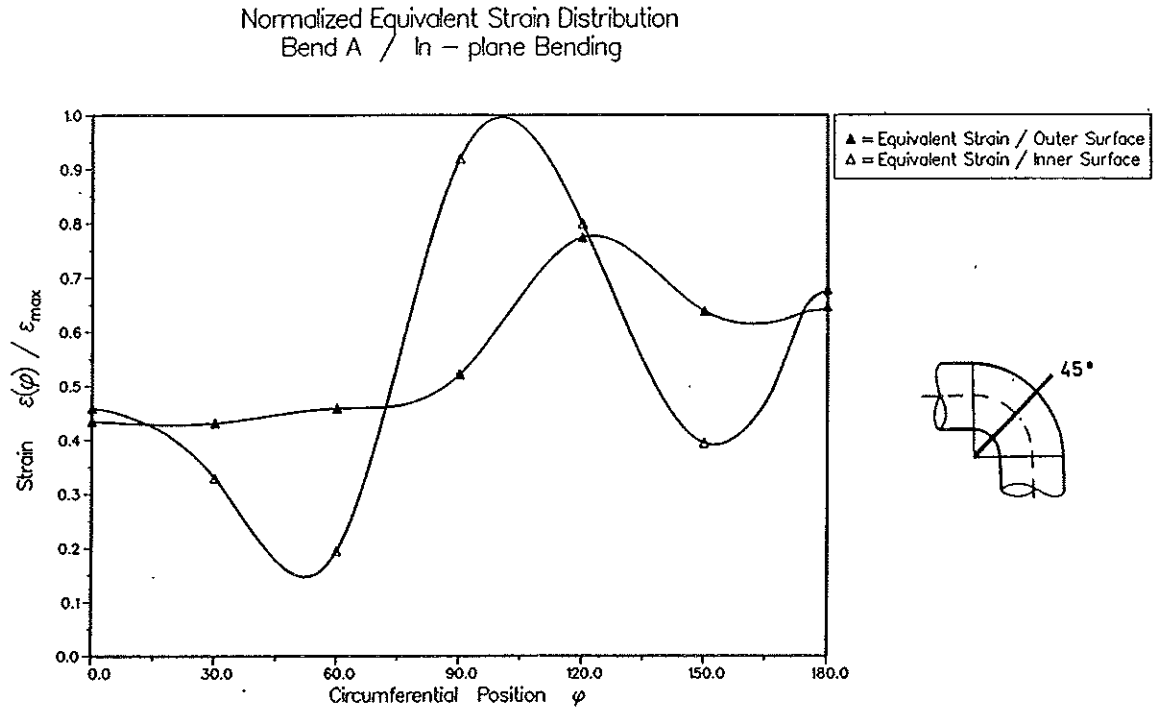

Fig. 3: Equivalent strain distribution of a thin-walled pipe bend, u = 1,16

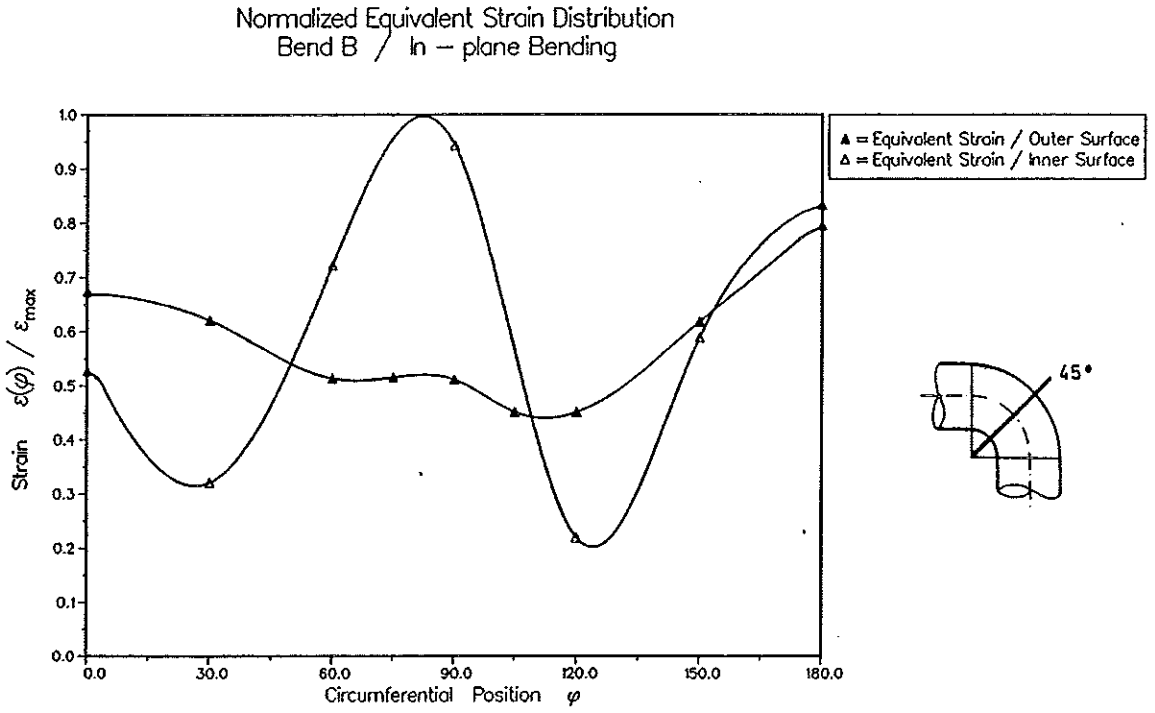

Fig. 4: Equivalent strain distribution of a pipe bend in the transition of thin- to thick-walled components, u = 1,21

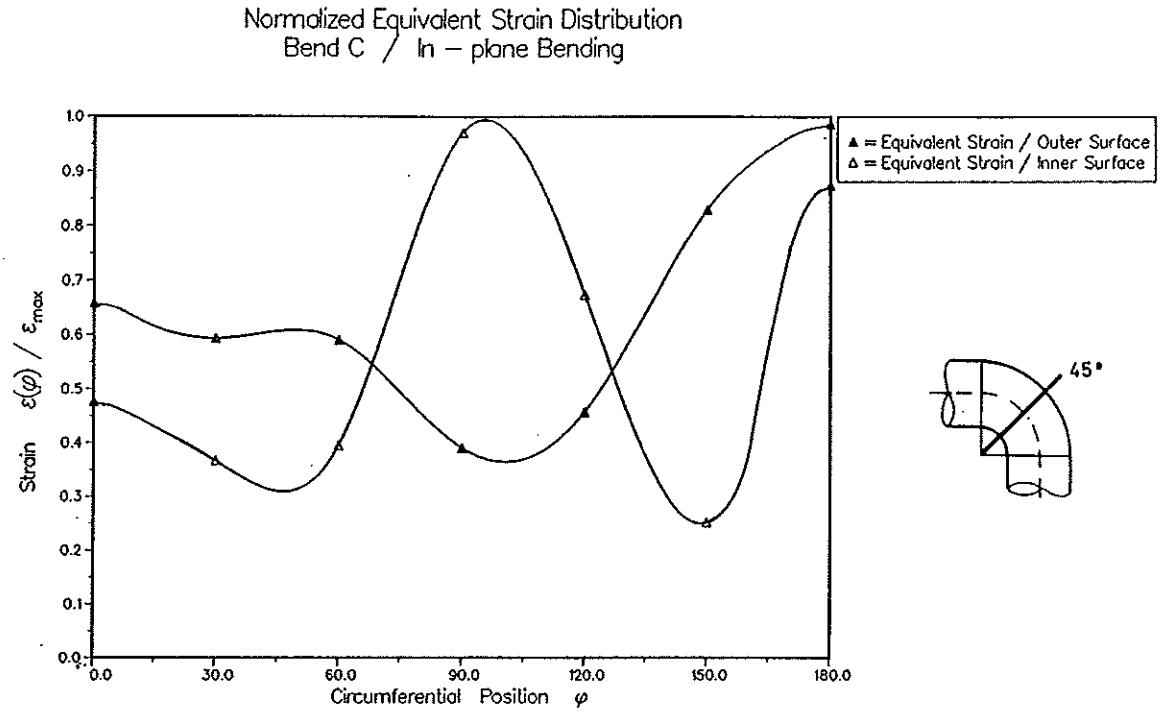

Fig. 5: Equivalent strain distribution of a thick-walled pipe bend, u = 1,39

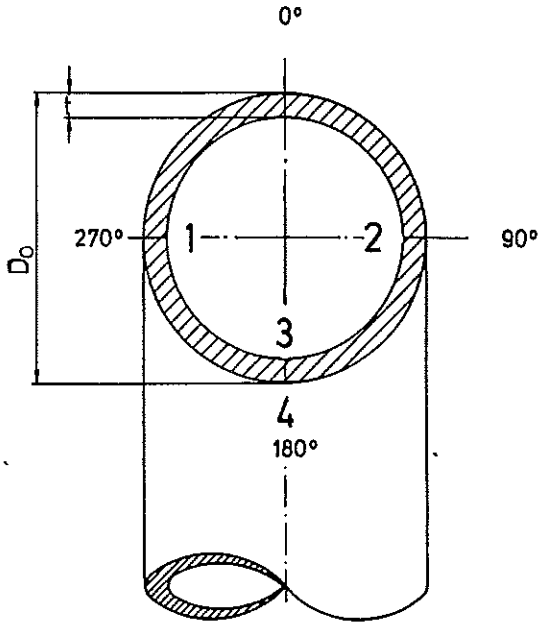

Position	1	2	3	4
Bend A	x	x		
Bend B	x	x	(x)	(x)
Bend C	x	x	(x)	x*

Fig. 6: Positions of incipient cracking at different pipe bend geometries

Staatliche Materialprüfungsanstalt

Universität Stuttgart

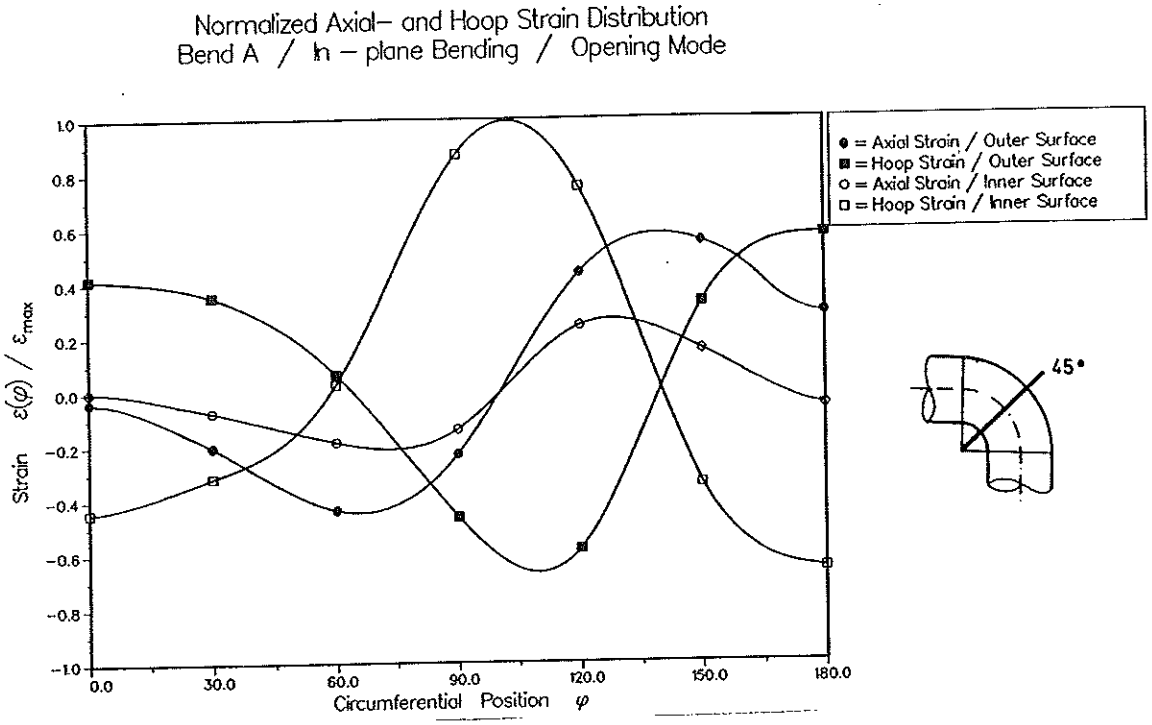

Fig. 7: Axial and hoop strain distribution of a thin-walled pipe bend, u = 1,16

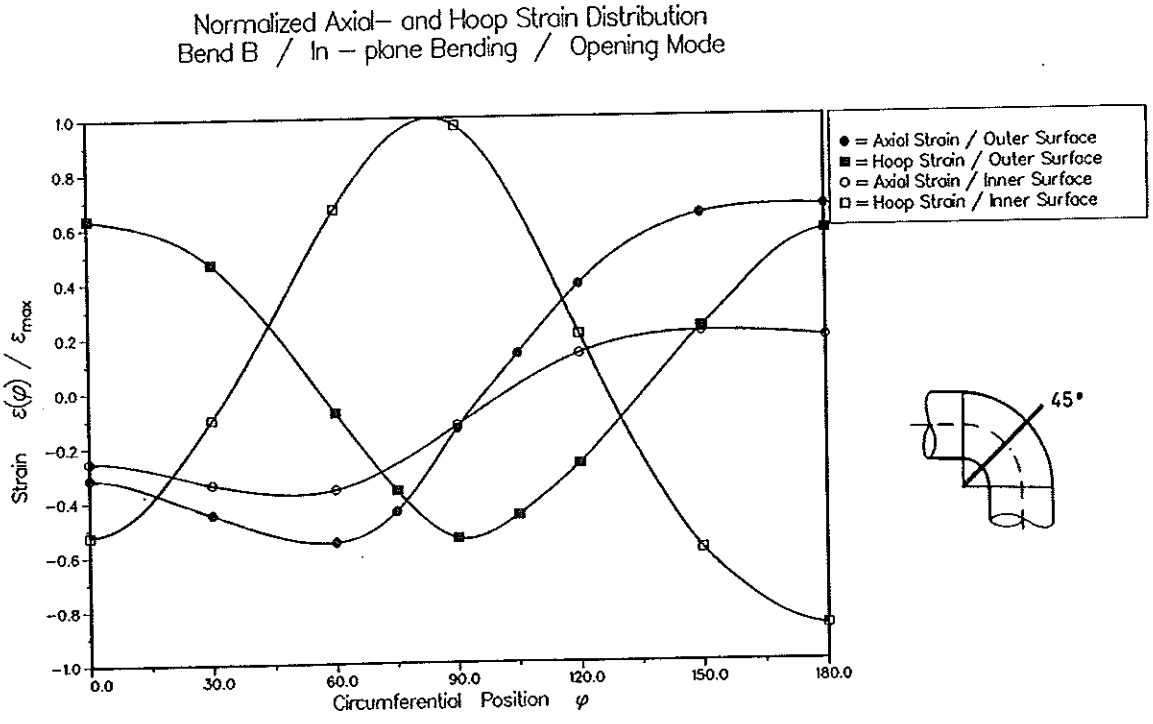

Fig. 8: Axial and hoop strain distribution of a pipe bend in the transition of thin- to thick-walled components, u = 1,21

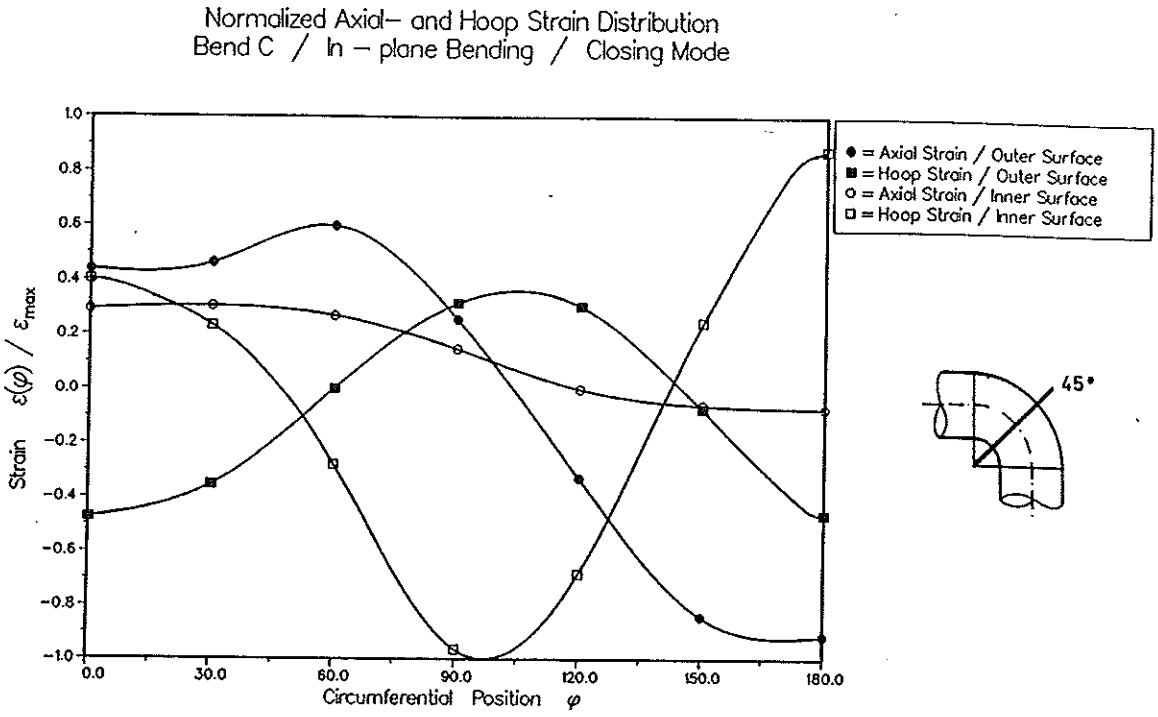

Fig. 9: Axial and hoop strain distribution of a thick-walled pipe bend, u = 1,39

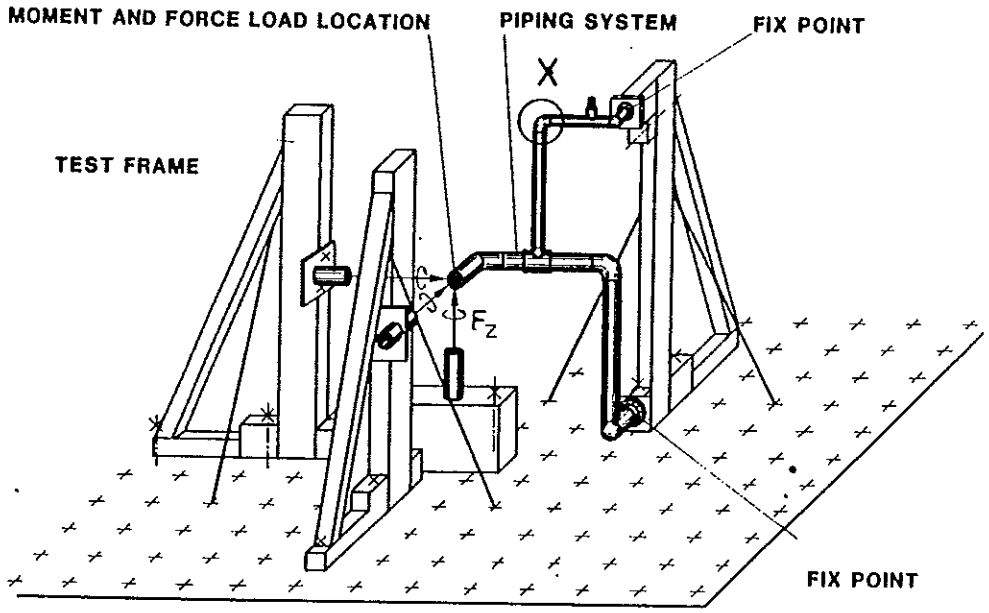

Fig. 10: Schematic representation of the pipe test rig

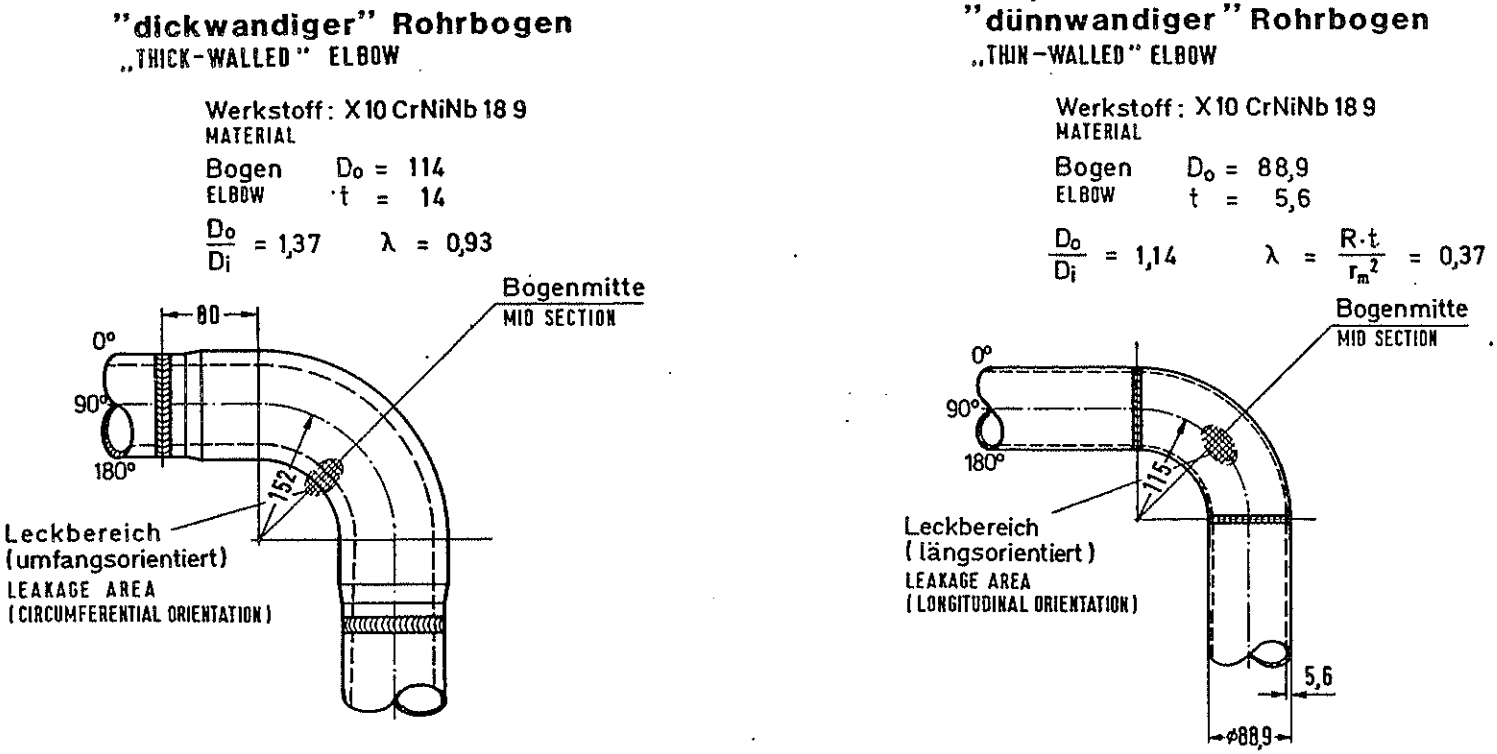

Fig. 11: Pipe bends under investigation in the fatigue tests

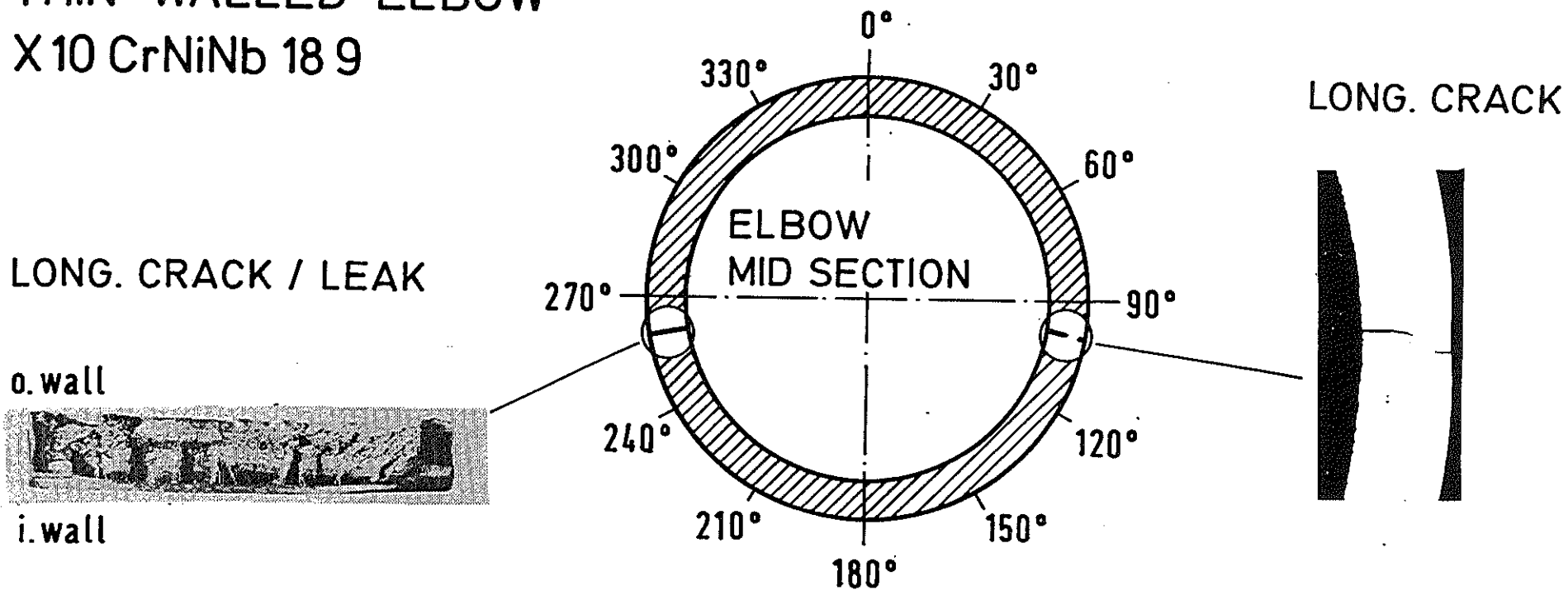

Fig. 12: Failure of a thin-walled elbow under cyclic in-plane bending

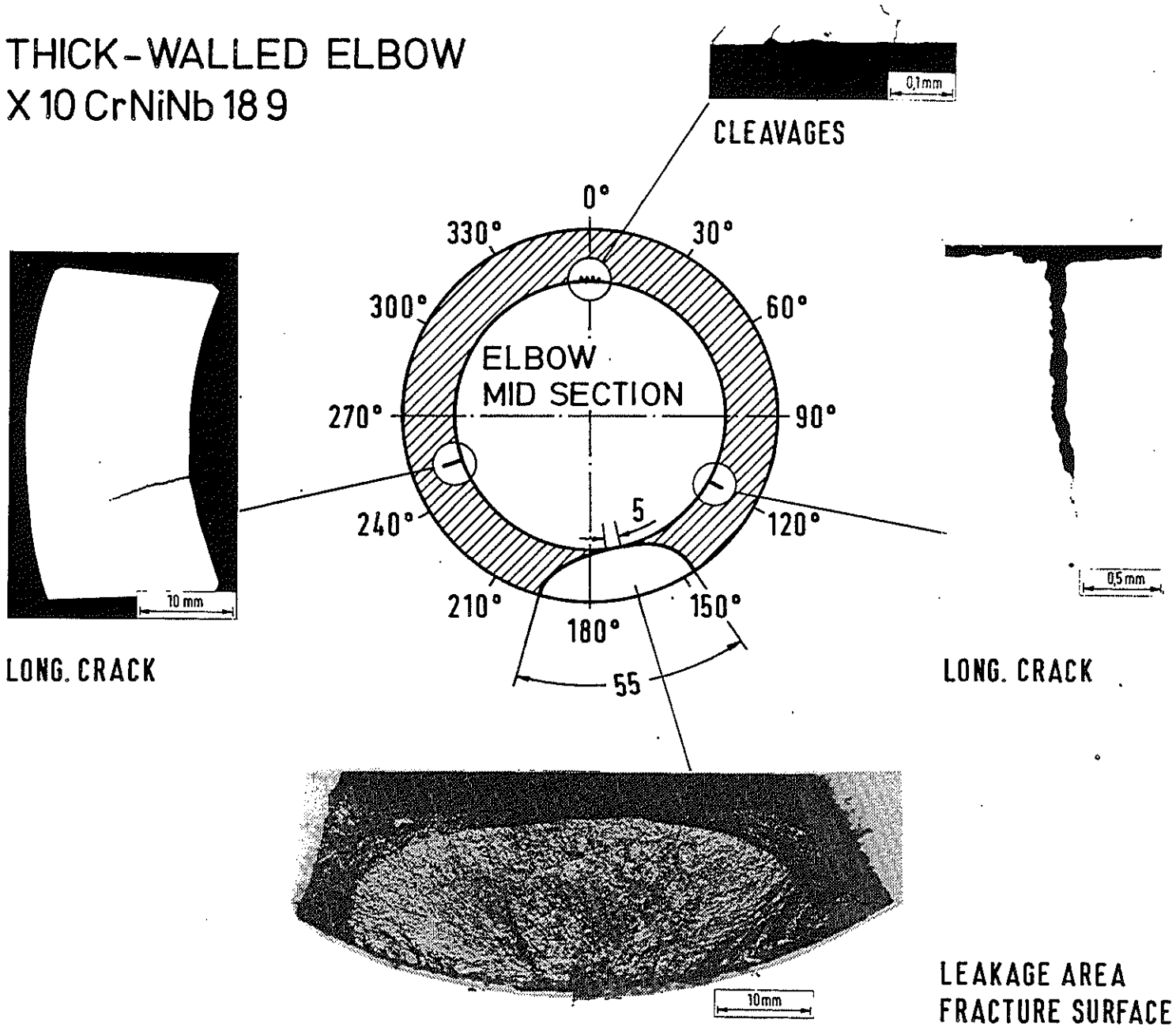

Fig. 13: Failure of a thick-walled elbow under cyclic in-plane bending

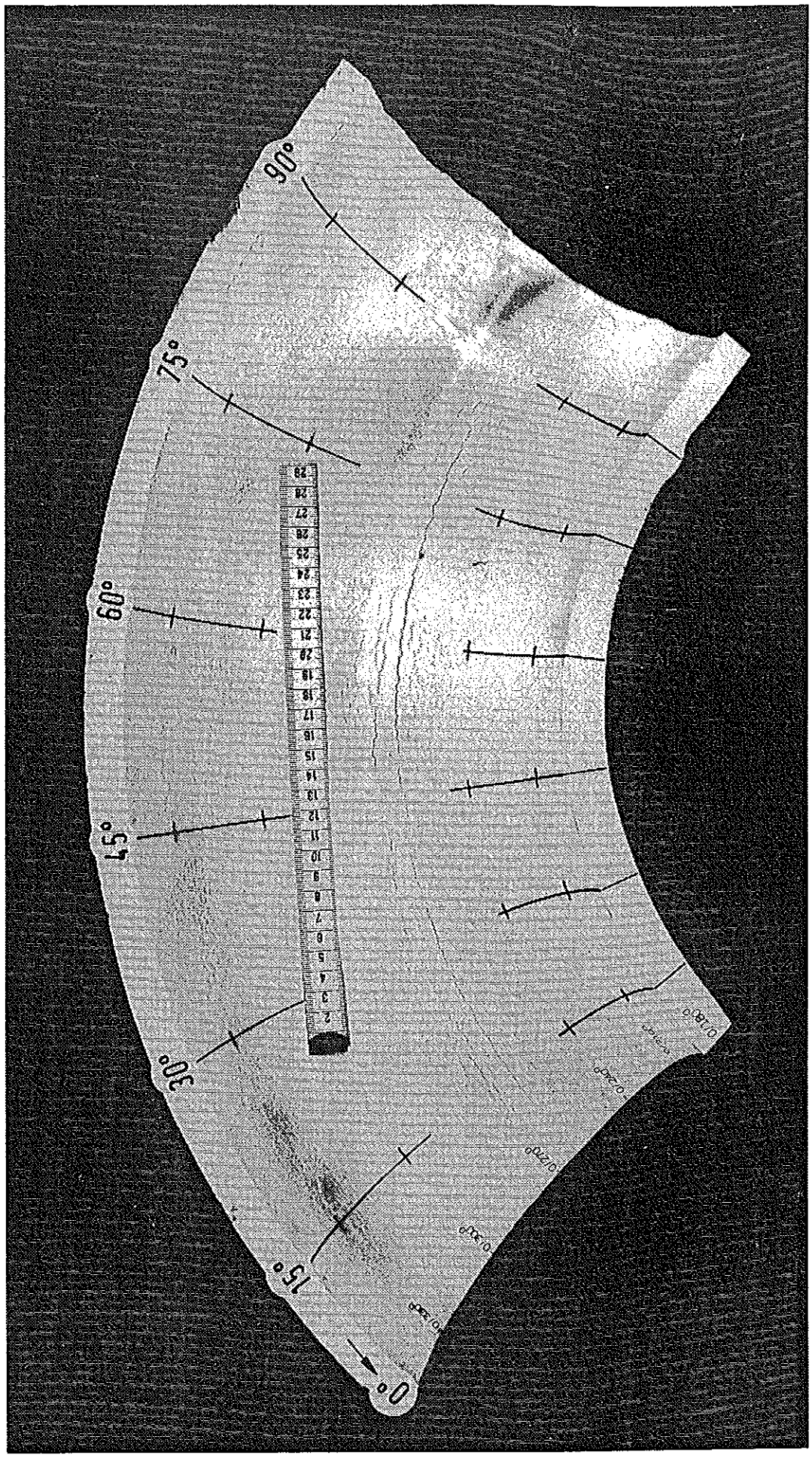

Fig. 14: Multiple cracking of a thin-walled elbow (DN 200) under in-plane bending /7/

**Staatliche
Materialprüfungsanstalt**

Universität Stuttgart

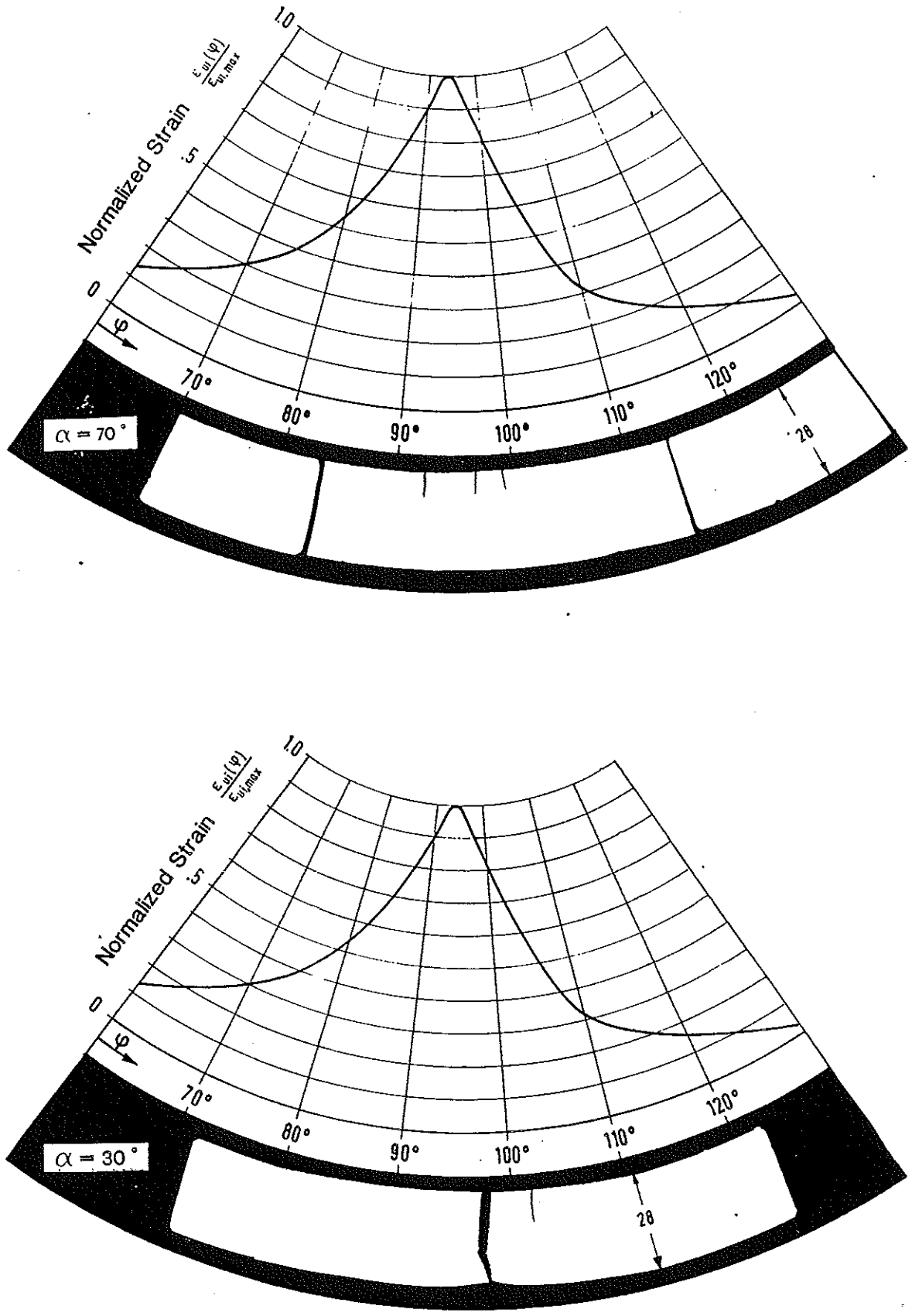

Fig. 15: Multiple cracking of a thin-walled elbow (DN 400) under in-plane bending /6/